ChemComm

Accepted Manuscript

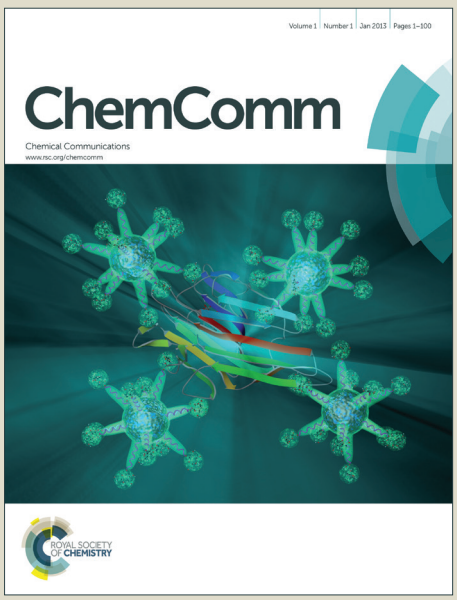

ROYAL SOCIETY OF CHEMISTRY

www.rsc.org/chemcomm

Chem Commun

RSCPublishing

COMMUNICATION

Morphological Self-Assembly of Enantiopure Allenes for Upstanding Chiral Architectures at Interfaces

Cite this: DOI: 10.1039/x0xx00000x

Yi-Qi Zhang,[a] Murat Anil Öner,[a] Inmaculada R. Lahoz,[b] Borja Cirera,[a] Carlos-Andres Palma,*[a] Silvia Castro-Fernández,[b] Sandra Míguez-Lago,[b] M. Magdalena Cid,[b] Johannes V. Barth,[a] José Lorenzo Alonso-Gómez,*[b] Florian Klappenberger*[a]

Received 00th January 2012,
Accepted 00th January 2012

DOI: 10.1039/x0xx00000x

www.rsc.org/

Chiroptically active allenes are employed for the construction of surface-confined nanostructures. Morphological complementarity between the homochiral units leads to self-assembly of highly ordered, upstanding architectures in two diastereomers. The novel, intertwined self-assembled monolayers feature reactive terminal alkynes for further functionalization and carry potential for widespread applications exploiting chiroptical amplification.

Chiral molecular systems at interfaces have attracted much attention in the last years[1] mainly due to their potential for enantioselective catalysis.[2] For the construction of such architectures, a most versatile approach is provided by the self-assembly of chiral organic molecules on achiral substrates.[1c, d] Scanning tunnelling microscopy (STM) is a useful tool to investigate surface-confined self-assembly of molecular architectures[3] and provides exquisite insight into the chiral properties of individual adsorbates[4] and complex superstructures.[5] The balance between substrate–molecule and molecule–molecule interactions along with the conformational freedom of the molecules determine the pertaining ordering scenarios.[3a, 6] Globally chiral surfaces can be constructed by employing enantiopure substances, chiral modifier doping, or chirality amplification by enantiomeric excess.[1c] With a dominating handedness these architectures also qualify for optical chirality sensing with great potential for applications.[7] However, the very weak or absent chiroptical responses of the employed species hamper their exploitation for real devices.

We have previously shown that cyclic and open allene oligomers feature outstanding chiroptical properties, which can be tuned by incorporation of aromatic units.[8] On the other hand, we explored the construction of 2D functional nanoarchitectures on surfaces,[3b, 9] and programmed supramolecular chirality into 2D networks by adequate functionalization.[10]

Herein, we employ for the first time a member of the allene family for the construction of chiral interfaces. The multifunctional (*M,M*)-**1** species (Fig. 1a) features a central pyridine unit, a versatile driving force for supramolecular structure formation via dipolar and π–π stacking interactions, connecting two chiral allene units responsible for large chiroptical activity. Furthermore, terminal alkynes represent an ideal framework for further functionalization via synthetic modification either in solution[11] or in situ.[12] When investigating the self-assembly of the multifunctional tecton on a noble metal fcc surface, we found chirality transfer from the building blocks into the monolayer-thin architectures in which molecules arrange regularly in an upstanding fashion. Since alignment control is a well-established approach for amplifying chiroptical responses, this upstanding chiral architecture (UCA) possesses an enormous potential for chiral sensing applications.[13]

The enantiopure (*M,M*)-**1** (Fig. 1a) was synthesized, purified and characterized as described in the Supporting Information (SI). The rotation of the terminal allene-di-tert-butyl-ethylene (ADTE) moieties (coloured in Fig. 1b) around the alkyne axis together with the bending of the alkyne axis results in extraordinary conformational flexibility. Despite averaging over all possible molecular conformations and orientations present in solution, a significant chiroptical activity is evidenced by the electronic circular

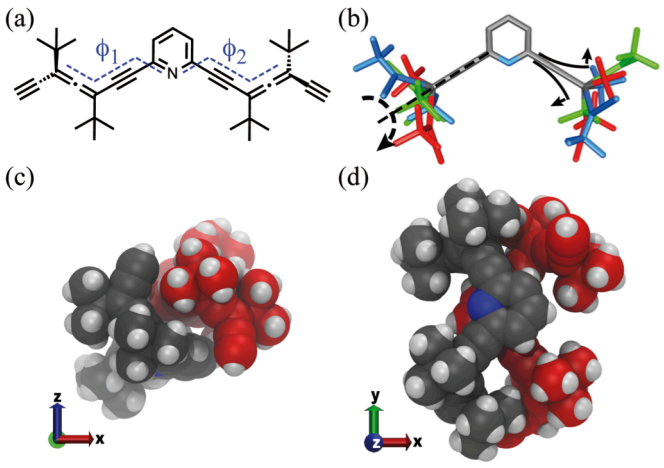

Fig. 1 (a) Chemical structure of (*M,M*)-**1** with definition of dihedral angles ϕ_1 and ϕ_2(blue). (b) Scheme of the conformational freedom (black arrows). Blue, green, and red moieties correspond to conformers with different values of ϕ_1 and ϕ_2. (c) Top and (d) side view of the intertwined dimer obtained from MD simulations.

dichroism (ECD) spectra (see Fig. S4). The structural and chiral stability after sublimation at 440 K and 10^{-6} mbar was certified by ^{1}H NMR and ECD spectroscopies.

The gas-phase properties of (*M,M*)-**1** were investigated with electrospray ionization mass spectrometry (ESI-MS). The spectrum (Fig. S7) indicates the presence of the intact monomer and a dimer of supramolecular nature. Surprisingly, the dimer signal strongly dominates over the monomer contribution. This clustering tendency remains even under very dilute conditions (Fig. S7-S10). These findings indicate that the molecule-molecule interactions are unusually strong for organic species of this size and type. It has to be mentioned, however, that both monomer and dimer signals indicate the presence of protonated species, which could contribute to the dimerisation preference.[14] For a better understanding of this assembly tendency, we investigated the agglomeration behaviour of unprotonated species via molecular dynamics (MD) simulations starting from 100 individual molecules in a volume corresponding to 10^{-4} M concentration (for details, see SI). After several ns-long simulations at 200 K we found a high probability for the formation of supramolecular dimers (Fig. S16), in agreement with the ESI-MS experiments. The most probable dimer conformation (Fig. 1c and d) is characterized by antiparallel-oriented pyridine stacking and complementarily intertwined ADTE groups inducing the impression of hugging molecules (Fig. S17). Each monomer has 29% (see SI, Fig. S21) of its van der Waals surface in contact with its counterpart. This percentage is near to the value (33%) obtained for a benzene ring adsorbed flat on a metal surface, which marks a typical contact surface of a flat-lying species. Therefore, our simulations suggest that the supramolecular assembly results from two driving forces. First, antiparallel stacking of the pyridine units aligns the centre of the organic units, and second, non-specific, intermolecular van der Waals attraction drives the optimisation of the molecule's morphology to allow a highly specific, shape-complementary packing mode which we term morphological self-assembly.

To explore the surface influence on the self-assembly of (*M,M*)-**1**, samples were prepared in ultra-high vacuum through organic molecular beam epitaxy on Ag(111) and investigated *in situ* by STM at 5.5 K (for more details see SI). A high-resolution STM image for a small molecular surface concentration reveals distinct clusters along with the underlying hexagonal atomic lattice (Fig. 2a). All the isolated objects appear as triangular features and preferentially adopt a registry such that the apparent height maxima are located at substrate hollow sites. Disrupt features in the centre of the image indicate that the organic units are easily displaced by the interaction with the tip. Often four-feature clusters are discernable (highlighted with dashed rhombs), which exhibit uniform shape and specific alignment with respect to the substrate high-symmetry directions.

Systematic molecule manipulations with the tip (Fig. 2b–e) demonstrate that two single-feature objects can be merged into a dimer and disassembled again in a reversible manner. The so-assembled dimers exhibit the same shape and alignment relative to the substrate directions as the original dimer (Fig. S11). We conclude that the dimers consist of two interacting (*M,M*)-**1** tectons and do not correspond to a different chemical species. Furthermore, with adapted manipulation parameters, dimers can be translated and rotated while keeping their integrity (see Fig. S12), indicating appreciable dimer stabilization. Based on these experiments, we conclude that each protrusion feature (with a single maximum) corresponds to a single (*M,M*)-**1** on Ag(111). As a consequence, dimeric aggregates and the four-feature clusters (highlighted with dashed rhombic cells, Figs. 2a) incorporate two and four (*M,M*)-**1** molecules, respectively.

For samples featuring a larger molecular coverage we found highly-ordered islands exhibiting borders that fit well into a parallelogram (Fig. 3a), indicating an assembly influenced by the substrate epitaxy. A zoomed-in image (Fig. 3b) demonstrates that the islands consist of periodically repeated rhombic units (highlighted in red) containing four protrusions each. At the borders less bright clusters with two (white) and rarely with three (green) protrusions are visible. The area of the rhombic units corresponds to that of the four-lobe clusters displayed in Fig. 2a. This agreement is a clear indication of the rhombic unit cell containing four molecules.

To determine the unit cell parameters, we analysed a large

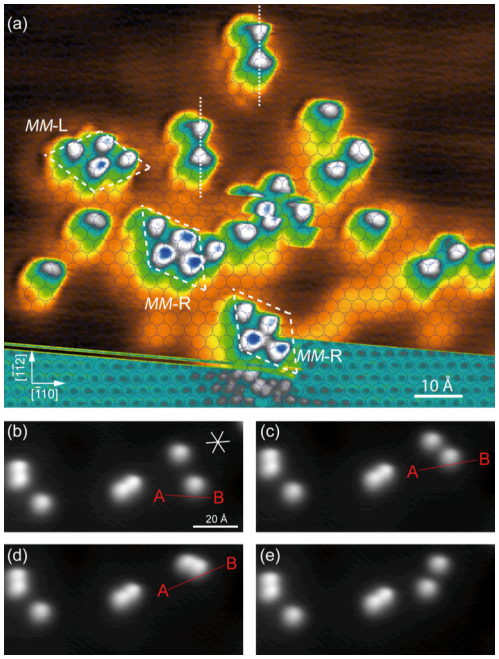

Fig. 2 (a) STM image of clusters of (*M,M*)-**1** on Ag(111) present for low molecular coverage. (U_B = 0.3V, I_T = 0.1 nA). (b-e) Tip manipulations of monomers and dimeric clusters. (U_B = 0.1 V, I_T = 0.1 nA).

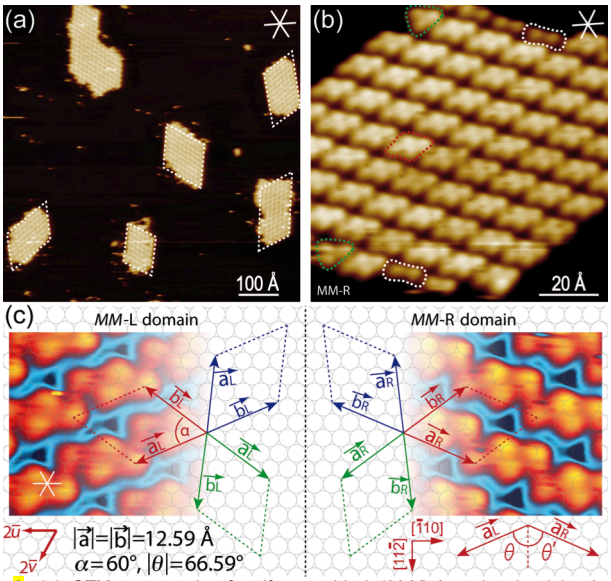

Fig. 3 (a) STM topograph of self-assembled (*M,M*)-**1** molecular islands on Ag(111) with surface high-symmetry directions (top-right). (b) Zoomed-in image of the regular superlattice with the tetrameric unit cell in red (U_B = −1.0 V, I_T = 0.05 nA). (c) Model of the architecture unit cells with proposed registry. Inset shows STM image in the same scale (U_B = −0.5 V, I_T = 0.1 nA).

number of STM images. Only two non-equivalent domain types, *MM*-L and *MM*-R (Fig. 3c and Fig. S13), were observed in a 1:1 ratio. Both types exist in three 120°-rotated, equivalent domains, as expected from the symmetry of the substrate. For the quantitative determination of the cell size, we averaged STM images of the same area obtained with four different slow-scan directions to minimize the influence of the thermal drift. As the substrate could be atomically resolved, the size of the unit cell and its relation with the underlying atomic lattice could be precisely identified (for details, see SI). Considering the dimensions of (*M,M*)-**1**, it is impossible to accommodate in a unit cell four molecules in a flat-lying geometry (see Fig. S14) without stacking molecules on top of each other. Consequently, the four molecules within a unit cell are proposed to adopt an upstanding orientation.

To understand why an upstanding, in contrast to a more intuitive flat-lying, adsorption geometry of the allene derivatives on the metal substrate is preferred, we performed MD simulations of four (*M,M*)-**1** units on a Ag(111) mimicking surface (for more details, see SI). This first set of low temperature calculations aims at investigating if for this family of molecules intermolecular attraction can dominate over molecule-substrate interaction rather than unravelling the exact geometry of an energy-optimised tetramer. Starting with two nearby dimers, each in the conformation depicted in Figs. 1c,d, the evolution of the tetramer geometry was followed during constant temperature (20 K) ns-long simulations. The energy-relaxed tetrameric cluster (Fig. 4a) consists of upstanding molecules only in which the dimers are recognizable by the antiparallel stacking of their pyridine rings. The average molecule–substrate van der Waals surface contact area is 9% (see SI), clearly qualifying this geometry as upstanding. The persistence of the tetramer against dissolving and reorienting to increase the metal-substrate contact area is a clear sign that the morphological drive behind the allene assembly is operational even in the presence of the metal surface. These findings are in full agreement with the experimental indications that the four-feature clusters depicted in Fig. 2a, consist of four upstanding molecules. For the simulated isolated tetramers (Fig. 4a), the ADTE intertwining at the top of one of the dimers was not observed despite

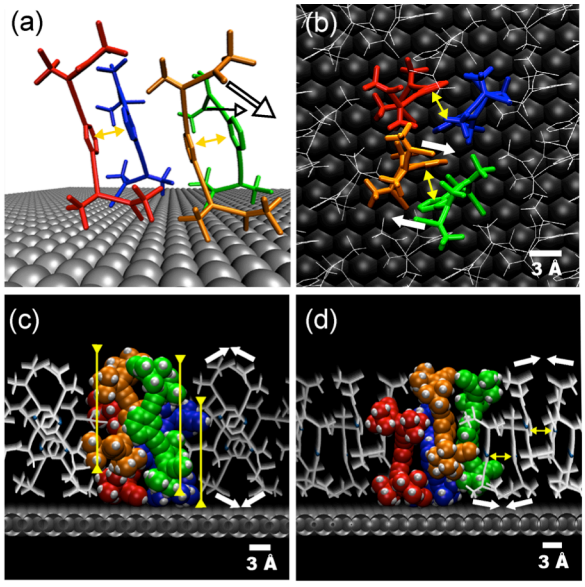

Fig. 4 (a) 3D rendering of an relaxed tetramer of (*M,M*)-**1** on a Ag(111)-mimicking substrate. (b) Top, (c) front, and (d) side view of the packing mode of the UCA according to MD simulations with periodic boundaries showing recovery of complementarily-packed ADTE groups (antiparallel white arrows). π-π stacking is indicated with yellow double arrows.

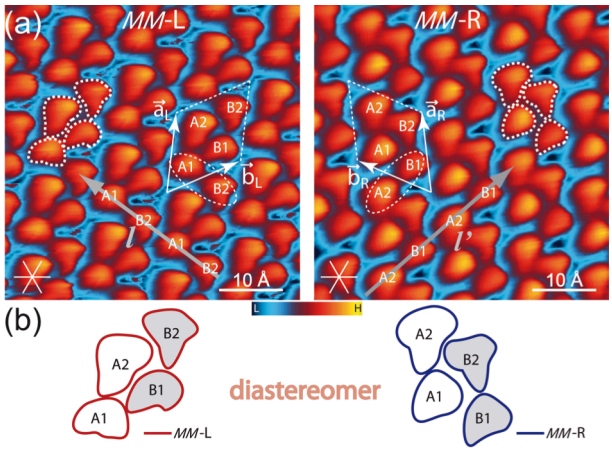

Fig. 5 (a) High-resolution STM images of *MM*-L (U_B = −0.3 V, I_T = 0.1 nA) and *MM*-R (U_B = −0.35 V, I_T = 0.05 nA) domains. Contours of single-molecule features depicted with dashed white curves. (b) Schematic representation of A1, A2, B1, and B2 contours of MM-L and MM-R domains forming diastereomers.

multiple MD runs, which can be seen from the ADTE groups showing a non-complementary orientation (black/white arrows pointing approximately in the same direction). This can be attributed to the low temperature used in the conformational search requiring forbiddingly long simulations to find global minima. Notably, the preference for assembling in isolated upright clusters contrasts the typical behaviour of alkene self-assembled monolayers (SAMs) of similar height[15] which require a coverage near to saturation to overcome the attraction towards the substrate.[16] Thus, allene UCAs seem better qualified for patterned and porous nanoarchitectures[17] because of well-defined tecton alignment even at the borders of the fabricated structures.

With the aim of unravelling the regular island structure, we performed further MD simulations with periodic boundary conditions at 200 K starting from the tetramer. Since in periodic boundary calculations denser geometries result in larger barriers for the molecular movement, especially changes of the conformation described by ϕ_1 and ϕ_2, we carried out simulations for slightly larger unit cells than experimentally observed, namely $a = b = 15$ Å, $\alpha = 60°$. This unit cell allows for full rotations of the ADTE moieties, resulting in the required sampling of the conformational space. As expected, after a few ns, low and high energy conformations can be sampled at equilibrium (see Fig. S20). Upon trajectory analysis, we find that in the lower energy tetramer configurations (cf. the snapshots of an energetically favourable situation depicted in Figs. 4b–d) the two dimers (orange-green and red-blue) are still recognisable via the π-stacked pyridine groups (yellow arrows), while no such interaction is indicated in between dimers. The molecules often exhibit complementary, embracing conformations resulting from antiparallel ADTE packing (white antiparallel arrows) at the top (orange-green dimer) or bottom (red-blue dimer) of the architecture. Thus, these configurations are reminiscent of the embrace found in the gas phase, the complementarity, however, is incomplete due to a wider range of exhibited conformations. The blue, green and orange molecule features $\phi_1 = \phi_2 \sim 0°$, ϕ_1 ~140° & $\phi_2 \sim 40°$, and $\phi_1 = \phi_2 \sim 140°$, respectively, resulting in units of different height (see yellow arrows in Fig. 4c). For efficient lateral packing optimising van der Waals interactions, one dimer (orange-green) is separated from the surface, allowing the bulky ADTE groups to reside at different altitude. Altogether, the MD studies strongly confirm the morphological self-assembly of the allene architecture on the Ag(111) surface. Please note that mutual conformational adaptation is an important concept in enantiospecific

recognition of peptides and has been tracked on the single-molecule level before.[18] In the peptide case, molecules adjust their conformation to allow or optimise site-selective interaction between specific functional moieties. In contrast, in our case non-directional and non-site-selective van der Waals interactions are responsible for the pronounced conformational adaptation rendering possible the highly shape-sensitive and enantiospecific molecular recognition taking place during the formation of the UCA.

The adsorption of an enantiopure compound, i.e., of a given handedness, onto enantiomeric interfacial unit cells providing a chiral footedness, should account for distinct diastereomeric molecule–substrate organisation.[1c, 19] Mirror-symmetric domains of the interfacial architecture can only be observed if the building blocks' handedness gets lost or interconverted. Both processes are possible in case the metal substrate would act catalytically. Thus, in order to study the transfer of chirality from the single-molecule level to the self-assembled architectures, we analysed high-resolution STM images of several islands obtained with the same tip and tunnelling parameters providing sharp molecular features (Fig. 5a). The shape of the features A1, A2, B1, and B2 is consistently repeated throughout both domains and, for clarity, highlighted (dashed) and extracted (Fig. 5b). Clearly, *MM*-L and *MM*-R domains do not exhibit mirror symmetry, thus are not enantiomeric. In both domains, the apparent height of the "A"-features exceeds that of the "B"-features (see line profiles in Fig. S15b). Both findings qualify the domains as diastereomers and confirm the transfer of chirality from the enantiopure allene (*M,M*)-**1** into the UCA, which accordingly is globally chiral.

We have achieved the construction of a complex, upstanding interfacial architecture from enantiopure allenes. Morphological self-assembly of the highly flexible species was found to play a crucial role in the formation of the novel chiral surfaces as ascertained by a combination of computational modelling, mass spectrometry, and molecular manipulation studies. Careful analysis of high-resolution STM images confirms the transfer of chirality from single molecules to overall chiral 2D networks. The use of enantiopure allenes with strong chiroptical responses, along with the post-synthetic modification possibilities of these UCAs, opens great possibilities for the construction of new smart materials that could be implemented into sensors or optically-driven logic gates.

We thank Xunta de Galicia (IPP contract J.L.A.G.) and Gobierno de España (CTQ2010–18576, and CTQ2011–28831) for financial support. Funding provided by the European Union via ERC Advanced Grant MolArt (No. 247299) is gratefully acknowledged. Manuel Marcos García is acknowledged for the careful mass spectrometry studies and Stefano Chiussi for the ultra-high vacuum tests.

Notes and references

[a] *Physik Department E20, Technische Universität München, James-Franck-Straße, 85748 Garching, Germany. E-mail: fklapp@ph.tum.de; c.a.palma@tum.de*

[b] *Departamento de Quimica Orgánica, Universidade de Vigo, 36310 Vigo, Spain. E-mail: lorenzo@uvigo.es.*

† Electronic supplementary information (ESI) available: Details of the synthesis, compound characterization, STM manipulation, and MD simulations. See DOI: 10.1039/c000000x/

1. (a) S. De Feyter, A. Gesquiere, M. M. Abdel-Mottaleb, P. C. M. Grim, F. C. De Schryver, C. Meiners, M. Sieffert, S. Valiyaveettil and K. Müllen, *Accounts Chem. Res.*, 2000, **33**, 520-531; (b) V. Humblot, S. M. Barlow and R. Raval, *Prog. Surf. Sci.*, 2004, **76**, 1-19; (c) K. H. Ernst, *Top. Curr. Chem.*, 2006, **265**, 209-252; (d) R. Raval, *Chem. Soc. Rev.*, 2009, **38**, 707-721.
2. (a) H. U. Blaser, *Tetrahedron: Asymmetry*, 1991, **2**, 843-866; (b) T. Mallat, E. Orglmeister and A. Baiker, *Chem. Rev.*, 2007, **107**, 4863-4890.
3. (a) J. V. Barth, *Annu. Rev. Phys. Chem.*, 2007, **58**, 375-407; (b) F. Klappenberger, *Prog. Surf. Sci.*, 2014, **89**, 1-55.
4. G. P. Lopinski, D. J. Moffatt, D. D. Wayner and R. A. Wolkow, *Nature*, 1998, **392**, 909-911.
5. (a) R. Fasel, M. Parschau and K. H. Ernst, *Angew. Chem. Int. Ed.*, 2003, **42**, 5178-5181; (b) J. A. A. W. Elemans, S. B. Lei and S. De Feyter, *Angew. Chem. Int. Ed.*, 2009, **48**, 7298-7332.
6. C.-A. Palma, M. Cecchini and P. Samorì, *Chem. Soc. Rev.*, 2012, **41**, 3713-3730.
7. (a) L. Pérez-Garcia and D. B. Amabilino, *Chem. Soc. Rev.*, 2002, **31**, 342-356; (b) G. A. Hembury, V. V. Borovkov and Y. Inoue, *Chem. Rev.*, 2008, **108**, 1-73; (c) C. Wolf and K. W. Bentley, *Chem. Soc. Rev.*, 2013, **42**, 5408-5424.
8. (a) J. L. Alonso-Gómez, P. Rivera-Fuentes, N. Harada, N. Berova and F. Diederich, *Angew. Chem. Int. Ed.*, 2009, **48**, 5545-5548; (b) S. Odermatt, J. L. Alonso-Gómez, P. Seiler, M. M. Cid and F. Diederich, *Angew. Chem. Int. Ed.*, 2005, **44**, 5074-5078; (c) P. Rivera-Fuentes, J. L. Alonso-Gómez, A. G. Petrovic, F. Santoro, N. Harada, N. Berova and F. Diederich, *Angew. Chem. Int. Ed.*, 2010, **49**, 2247-2250; (d) J. L. Alonso-Gómez, P. Schanen, P. Rivera-Fuentes, P. Seiler and F. Diederich, *Chem. Eur. J.*, 2008, **14**, 10564-10568.
9. (a) R. Decker, U. Schlickum, F. Klappenberger, G. Zoppellaro, S. Klyatskaya, M. Ruben, J. V. Barth and H. Brune, *Appl. Phys. Lett.*, 2008, **93**, 243102-1-3; (b) J. V. Barth, *Surf. Sci.*, 2009, **603**, 1533-1541; (c) D. Kühne, F. Klappenberger, W. Krenner, S. Klyatskaya, M. Ruben and J. V. Barth, *Proc. Natl. Acad. Sci. U.S.A.*, 2010, **107**, 21332-21336; (d) W. Krenner, F. Klappenberger, D. Kühne, K. Diller, Z.-R. Qu, M. Ruben and J. V. Barth, *J. Phys. Chem. Lett.*, 2011, **2**, 1639-1645; (e) F. Klappenberger, D. Kühne, W. Krenner, I. Silanes, A. Arnau, F. J. García de Abajo, S. Klyatskaya, M. Ruben and J. V. Barth, *Phys. Rev. Lett.*, 2011, **106**, 026802-026802.
10. S. Stepanow, N. Lin, F. Vidal, A. Landa, M. Ruben, J. V. Barth and K. Kern, *Nano Lett.*, 2005, **5**, 901-904.
11. (a) C. Glaser, *Ber. Dtsch. Chem. Ges.*, 1869, **2**, 422-424; (b) R. Huisgen, G. Szeimies and L. Möbius, *Chem. Ber.-Recl.*, 1967, **100**, 2494-2507.
12. Y.-Q. Zhang, N. Kepčija, M. Kleinschrodt, K. Diller, S. Fischer, A. C. Papageorgiou, F. Allegretti, J. Björk, S. Klyatskaya, F. Klappenberger, M. Ruben and J. V. Barth, *Nat Commun*, 2012, **3**, 1286-1-8.
13. (a) A. Guerrero-Martínez, B. Auguié, J. L. Alonso-Gómez, Z. Džolić, S. Gómez-Graña, M. Žinić, M. M. Cid and L. M. Liz-Marzán, *Angew. Chem. Int. Ed.*, 2011, **50**, 5499-5503; (b) H. S. Oh, H. Jee, A. Baev, M. T. Swihart and P. N. Prasad, *Adv. Funct. Mater.*, 2012, **22**, 5074-5080; (c) K. Watanabe, K. Suda and K. Akagi, *J. Mater. Chem. C*, 2013, **1**, 2797-2805.
14. I. K. Attah, S. P. Platt, M. Meot-Ner, M. S. El-Shall, S. G. Aziz and A. O. Alyoubi, *J. Chem. Phys.*, 2014, **140**, 114313.
15. F. Schreiber, *Prog. Surf. Sci.*, 2000, **65**, 151-256.
16. F. Schreiber, A. Eberhardt, T. Y. B. Leung, P. Schwartz, S. M. Wetterer, D. J. Lavrich, L. Berman, P. Fenter, P. Eisenberger and G. Scoles, *Phys. Rev. B*, 1998, **57**, 12476-12481.
17. R. K. Smith, P. A. Lewis and P. S. Weiss, *Prog. Surf. Sci.*, 2004, **75**, 1-68.
18. M. Lingenfelder, G. Tomba, G. Costantini, L. Colombi Ciacchi, A. De Vita and K. Kern, *Angew. Chem. Int. Ed.*, 2007, **46**, 4492-4495.
19. M. Forster, M. S. Dyer, M. Persson and R. Raval, *J. Am. Chem. Soc.*, 2011, **133**, 15992-16000.

